Weierstraß-Institut
für Angewandte Analysis und Stochastik

im Forschungsverbund Berlin e.V.

High resolution fMRI: Overcoming the Signal-To-Noise Problem

Karsten Tabelow[1] [4], Valentin Piëch[2], Jörg Polzehl[1], Henning U. Voss[3]

submitted: 27th August 2008

[1]   Weierstrass Institute
    for Applied Analysis and Stochastics
    Mohrenstr. 39
    10117 Berlin, Germany
    E-Mail: `tabelow@wias-berlin.de`

[2]   Laboratory of Biological Modelling
    Rockefeller University
    New York, NY, USA

[3]   Citigroup Biomedical Imaging Center
    Dept. of Radiology
    Weill Cornell Medical College
    New York, NY, USA

No. 1353

Berlin 2008

Abstract

Increasing the spatial resolution in functional Magnetic Resonance Imaging (fMRI) inherently lowers the signal-to-noise ratio (SNR). In order to still detect functionally significant activations in high-resolution images, spatial smoothing of the data is required. However, conventional non-adaptive smoothing comes with a reduced effective resolution, foiling the benefit of the higher acquisition resolution. We show how our recently proposed structural adaptive smoothing procedure for functional MRI data can improve signal detection of high-resolution fMRI experiments regardless of the lower SNR. The procedure is evaluated on human visual and sensory-motor mapping experiments. In these applications, the higher resolution could be fully utilized and high-resolution experiments were outperforming normal resolution experiments by means of both statistical significance and information content.

1 Introduction

Functional Magnetic Resonance Imaging (fMRI) has become the most informative tool for in-vivo examination of human brain function on small spatial scales. It is nowadays utilized both in research as well as in clinical applications such as diagnosis and treatment of brain lesions. Now that fMRI reached a spatial resolution of about a millimeter and thus approaches a fundamental organizational scale of brain functions, namely cortical columns, it is expected that pushing the technique to higher resolutions will provide even improved insights into brain function in the near future. However, high-resolution fMRI has an intrinsically lower signal-to-noise ratio (SNR) than lower resolution methods, entailing challenges on experimental setup as well as on data analysis. A significant recent discussion in this Journal [Kriegeskorte and Bandettini, 2007a, Kleinschmidt, 2007, Kriegeskorte and Bandettini, 2007b] showed the importance of addressing these questions in a systematic way.

Since MRI image SNR is proportional to the sample volume per image voxel [Edelstein et al., 1986], the signal detection situation is impaired at higher spatial resolution. In order to enhance signal detection and to weaken the severe multiple test problem, spatial smoothing is common [Forman et al., 1995, Lowe and Sorenson, 1997]. However, the application of conventional, non-adaptive smoothing methods such as Gaus-

sian filters leads to an effective spatial resolution that is comparable to the situation when the data is acquired at a lower spatial resolution but better SNR. One could therefore conclude that it is better to acquire fMRI data at lower resolutions [Scouten et al., 2006] due to the inherent SNR loss at higher resolutions. Since physiological noise is proportional to the signal strength, which in turn decreases with decreasing voxelsize, the situation at higher resolutions could possibly be improved beyond previously described physics-based limits [Triantafyllou et al., 2006]. Nonetheless, conventional data smoothing is intrinsically not suitable as a technique to utilize the benefits of higher resolution. Therefore, a smoothing procedure would be desirable that does not lower the effective resolution but nevertheless provides enhanced signal detection capabilities. Recently, we proposed such a structural adaptive smoothing method based on the Propagation Separation (PS) approach [Tabelow et al., 2006, Tabelow et al., 2008], which overcomes the drawbacks of non adaptive smoothing. The same intention inspired [Harrison et al., 2007, Harrison et al., 2008] to use spatial priors derived from the Laplace-Beltrami diffusion framework.

In this contribution we will show that with using our smoothing method the potential of functional imaging at higher resolution can be more fully utilized, which is demonstrated on a visual localizer experiment and a sensory-motor experiment. In both experiments we find that high-resolution scanning combined with structural adaptive smoothing clearly outperforms no smoothing and Gaussian smoothing, and that the proposed procedure enables one to take better advantage of high-resolution scanning. We believe that the use of appropriate filtering techniques can make not only research studies more powerful but also render clinical applications more informative, by increasing resolution without exceeding clinically serviceable scan times.

2   Signal-to-noise ratio in fMRI

The determination of signal-to-noise ratio (SNR) in fMRI and its comparison between experiments with differing resolution and other acquisition parameters is a non-trivial task, both from a theoretical as well as from an experimental view. The main reason is that the SNR depends on various parameters and conditions that often cannot be easily held constant through different experimental settings. Another reason is that SNR depends on physical as well as on physiological parameters, the latter one being more complex and less well understood than the former. The main issues of SNR in fMRI can be summarized as follows:

Noise in functional MRI can be well described by a sum of uncorrelated Gaussian distributions of image noise of physical origin (σ_0) and physiological contributions

(σ_P) [Krüger and Glover, 2001]. Thus, the SNR, in particular in fMRI often denoted as "time course SNR" [Triantafyllou et al., 2005, Triantafyllou et al., 2006], is given by

$$SNR = \frac{S}{\sqrt{\sigma_0^2 + \sigma_P^2}} , \tag{1}$$

where S is the measured signal intensity in any one voxel. Since the physiological component σ_P of the noise approximately scales with the signal size, i.e., $\sigma_P = \lambda S$ [Krüger and Glover, 2001], one has

$$
\begin{aligned}
SNR & = \frac{S}{\sqrt{\sigma_0^2 + \lambda^2 S^2}} \\
& = \frac{SNR_0}{\sqrt{1 + \lambda^2 SNR_0^2}}
\end{aligned}
$$

with the image signal-to-noise ratio $SNR_0 = S/\sigma_0$. Hence,

$$SNR = \frac{1}{\sqrt{SNR_0^{-2} + \lambda^2}} . \tag{2}$$

If FOV_x and FOV_y denote the field-of-view in x- and y-direction, respectively, N_x and N_y the acquisition matrix size in phase and frequency direction, respectively, $\Delta x = FOV_x/N_x$, $\Delta y = FOV_y/N_y$, and Δz the three voxel dimensions, BW the frequency bandwidth, and N_{av} the number of averages, the image SNR is given by [Edelstein et al., 1986, Parker and Gullberg, 1990, Sijbers, 1998]

$$SNR_0 = \kappa \, V \, \sqrt{\frac{N_{av} N_x N_y}{BW}} , \tag{3}$$

with the voxel volume $V = \Delta x \Delta y \Delta z$. The parameter κ is the proportionality factor between signal size and voxel volume, and depends on the sample properties and acquisition parameters such as echo and repeat times. Note, that in the case of non-interleaved excitation the scan time is given by $N_{av} \cdot TR \cdot N_y$. Let us consider $N_{av} = 1$ and $BW = 1$ in arbitrary units. Thus, we have

$$SNR = \frac{1}{\sqrt{\kappa^{-2} V^{-2} N_x^{-1} N_y^{-1} + \lambda^2}} \tag{4}$$

which reduces to $SNR = \kappa V \sqrt{N_x} \sqrt{N_y} = SNR_0$ in case of absence of physiological noise ($\lambda = 0$). Due to the two dimensional image acquisition, we henceforth assume a constant slice thickness Δz.

Within these specifications we compare the SNR in acquisitions with a low and a high spatial resolution. If for the low resolution acquisition we set $V = 1$ in arbitrary units and $N_x = N_y = 64$, we have

$$SNR_{low}^{-1} = \sqrt{\kappa^{-2}/4096 + \lambda^2} . \tag{5}$$

3

#	Δx	Δy	V	N_x	N_y	FOV_x	FOV_y	Time	SNR^{-2}	nSNR$_0$
1.	1	1	1	64	64	64	64	1	$\kappa^{-2}/4096 + \lambda^2$	1
2.	0.5	0.5	0.25	256	256	128	128	4	$\kappa^{-2}/4096 + \lambda^2$	1
3.	0.5	0.5	0.25	128	128	64	64	2	$\kappa^{-2}/1024 + \lambda^2$	0.5
4.	0.5	0.5	0.25	64	64	32	32	1	$\kappa^{-2}/256 + \lambda^2$	0.25
5.	1	1	1	128	128	128	128	2	$\kappa^{-2}/16384 + \lambda^2$	2

Table 1: Signal-to-noise ratio (SNR) and scan time for various acquisition resolutions and fields-of-view (FOV), assuming free choice of other imaging parameters calculated from Eq. (4). All other imaging parameters are assumed constant. The numbers for nSNR$_0$ in the rightmost column represent the SNR as normalized to the first row of the table and as would be measured in phantoms, i.e., without physiological noise components ($\lambda = 0$). All values are given in arbitrary units.

A high resolution scan with twice the resolution in both in-plane dimensions would then result in a voxel volume $V = 0.25$. There are two possibilities to achieve doubled resolution, with different effects on the SNR (see Table 1): shrinking the field-of-view and increasing the matrix size. We do not discuss here, nor is it important for the results, when or whether these alternatives are meaningful. We simply point to the fact that the first two rows of Table 1 result in the same SNR. However, this comes at the cost of quadrupled scan time! Furthermore, as indicated in the last row of Table 1, for each low resolution scan, there is a parameter setting yielding the same resolution but a doubled SNR in case of no physiological noise. Not all settings can always be realized in two acquisitions with different parameters for the same experiment, since scan time and sample coverage are effected by the choice of resolution as well.

Shrinking the field-of-view inherently comes with a loss of SNR [Edelstein et al., 1986, Scouten et al., 2006] using the same scan time. This can be seen in the fourth row of Table 1 as compared to the first row, where with the same matrix size but half field-of-view as in the low resolution acquisition the SNR at the higher resolution is only one quarter of the low resolution scan, in absence of physiological noise ($\lambda = 0$). Therefore, for the experiments described in this paper, we achieve higher resolution by only increasing the matrix size keeping the field-of-view constant, although this strategy increases the scan time or, alternatively, reduces coverage. One could now argue that this comparison between a lower and a higher resolution is misleading since it somehow hides the costs for achieving a higher spatial resolution with passable SNR. There are three reasons for us doing so. First, it is a natural setting, if one is interested in a high spatial resolution for a given field-of-view. Second, for the main result of this paper, namely the achievement of structural adaptive smoothing in high resolution fMRI, the specific settings are not

relevant, since the smoothing bandwidth of the algorithm can be chosen in a completely different way as for common Gaussian filtering. This will be discussed in detail in the next section. Third, the presence of physiological noise may improve the situation in favor of the high resolution scan. Physiological noise cannot be neglected [Krüger and Glover, 2001], especially at higher field strength of 3.0 T or above. According to Eq. (4), the loss in SNR of acquisition 3 relative to acquisition 1 in Table 1 is less than 2 for $\lambda > 0$. Note, that when comparing acquisitions 1 and 4 the loss is less than 4. Figure 1 illustrates SNR-ratios as functions of $\kappa\lambda$ for the acquisition schemes in Table 1.
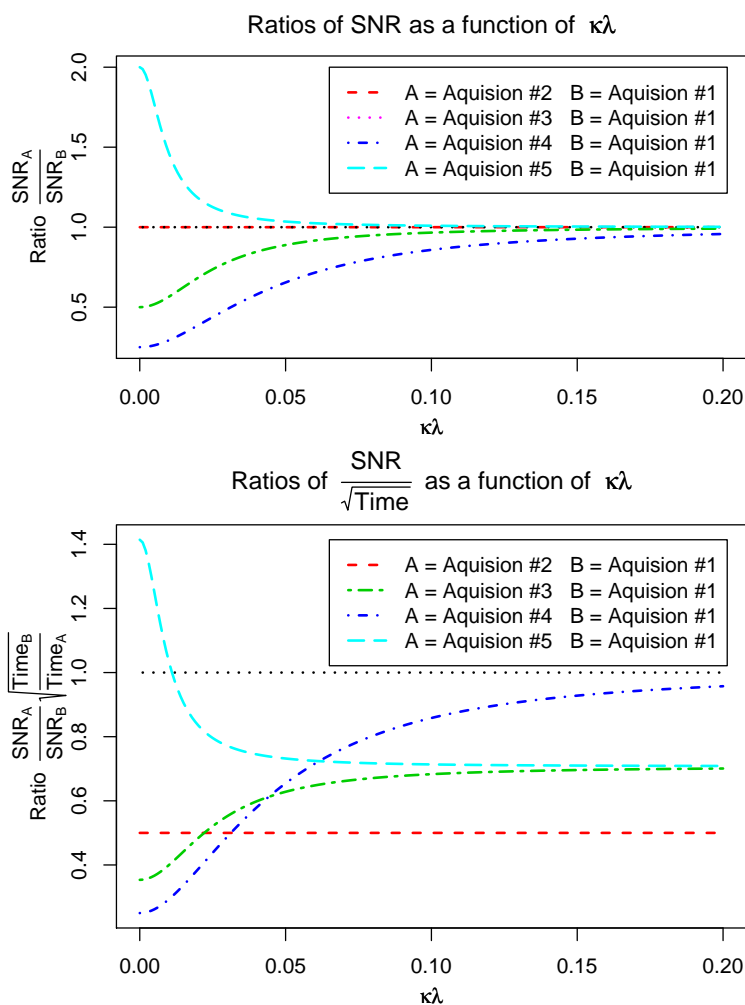

Figure 1: Ratios between SNR's (top) and SNR's standardized by square root of acquisition times (bottom) of acquisitions # 2 — 5 and acquisition # 1 as a function of $\kappa\lambda$.

3 Smoothing fMRI data

The loss in SNR at high resolutions can be compensated to some degree by smoothing. Smoothing is advised generally if at least one of two conditions hold: First, the BOLD-signals are weak such that they cannot be detected without smoothing. Second, random field theory is used to correct for the multiple testing problem; in random field theory, defining the thresholds for signal detection requires a certain amount of smoothness for the assumptions of random field theory to be valid. This corresponds to the challenges 2 and 3 discussed in [Kriegeskorte and Bandettini, 2007a], which are especially important at higher resolutions. However, non-adaptive smoothing inherently reduces the effective resolution with significant blurring at borders of activation areas. Thus, the advantages of high resolution scanning are diminished to some degree. If one is interested in functional structures at higher spatial resolution, one is caught in a trap: The SNR at the high resolution may be too low and the multiple test problem may be too severe, leaving no multiple test-corrected activations. Non-adaptive smoothing weakens the multiple test problem and increases the SNR, but lowers the effective resolution, such that one can argue that a lower resolution scan with increased SNR is advisable [Scouten et al., 2006].

Recently, we proposed a structural adaptive smoothing procedure [Tabelow et al., 2006], that overcomes the drawbacks of non-adaptive smoothing and can achieve a noise reduction without blurring the borders and thus keeping the effective resolution of the functional image as acquired in the scan. Here, we shortly review the main properties of our algorithm and restrict ourselves to the case of BOLD fMRI experiments and analysis by a linear model [Friston et al., 1995, Worsley and Friston, 1995, Worsley et al., 2002]. One could easily translate the application of structural adaptive smoothing to other contexts, which is beyond the scope of this paper.

Our approach for smoothing fMRI data is mainly based on the observation that the structures of interest are defined by areas in which the parameter values corresponding to the BOLD signal are similar and differ significantly from zero. The common non-adaptive filtering approaches smooth the data cube at each time step separately, without making use of the information contained in the time series. We therefore suggested to first evaluate the linear model

$$Y_i = X\beta_i + \varepsilon_i \tag{6}$$

for the time series $Y_i = (Y_{it})_{t=1...T}$ at each voxel i [Tabelow et al., 2006]. The design matrix X contains the expected BOLD response evaluated at scan acquisition times and nuisance parameters such as a slowly varying drift. After performing some appropriate

prewhitening procedure, the error vector $\varepsilon_i = (\varepsilon_{it})_{t=1...T}$ can be assumed to have zero expectation and to be approximately uncorrelated.

We obtain fields of least squares estimates $\widehat{\beta}_i$ for the parameter value β_i and, what is most important, its error variance $\mathrm{Var}\,\widehat{\beta}_i$. Both fields are used in our structural adaptive smoothing procedure. First, we define a structural assumption, which should be valid for the field of the true parameter β_i. In non-activated areas the parameter value is zero, while it differs from zero in areas which are activated during the scan. In activated areas the parameter values are similar. Hence, our structural assumption is a local constant model for the BOLD-parameter. Based on this assumption, we developed an iterative smoothing algorithm for the statistical parametric map (SPM) that is based on pairwise tests of homogeneity [Tabelow et al., 2006]. The result is a smoothed SPM where the shape and borders of the activation structure is preserved. As a consequence, in contrast to other non-adaptive smoothing methods, the procedure does reduce noise while preserving the resolution of the scan.

The main parameter of our procedure, which can be defined by the user, is the maximum achievable variance reduction or equivalently a maximum achievable smoothness. Both can be specified by selecting a maximum bandwidth [Tabelow et al., 2006]. While over-smoothing is avoided through construction in the algorithm as long as differences between the parameter values of two such region are statistically significant, the largest homogeneous region is to be expected the non-activation area, where the parameter value does not significantly differ from zero. We therefore can choose the maximum bandwidth much larger than in non-adaptive smoothing (as defined by the matched filter theorem) and achieve a larger amount of variance reduction without blurring. This has the effect of lowering the thresholds for signal detection, since the smoothness in non activation areas, which determine the threshold under the hypothesis of no signal, is directly proportional to the bandwidth. We therefore expect our procedure to be efficient in particular at higher resolutions.

To summarize the last two sections, we consider the problem of signal detection at a low and a corresponding high resolution scan. While smoothing the high resolution scan with common non-adaptive tools may not be able to recover the SNR even at the effective resolution of the low resolution scan, our adaptive procedure does reduce the noise and hence increases the SNR at the acquisition resolution. Thus, we directly tackle the challenges 2 and 3 mentioned in [Kriegeskorte and Bandettini, 2007a] at the desired high resolution. In the rest of the paper we demonstrate this for artificial as well as experimental data.

4 Examples

4.1 Artificial data

For the creation of an artificial dataset we use the numerical phantom from one of our previous publications [Tabelow et al., 2008]. Here, we analyze this phantom at different spatial resolutions. The basic artificial dataset consists of $64 \times 64 \times 26$ voxels. A slice containing activation is replicated three times in the z-direction, followed by two slices with no activation. Voxel size in z-direction was specified as twice the voxel size within slices. At each of these voxels a time series was created with 107 samples, stimulus onset times at the 18th, 48th, and 78th sample with a stimulus duration of 15 samples and 2 s between two samples. The positions of activated regions within the slices and the amplitudes of the signal are illustrated in Fig. 2.

The form and size of activation areas change radially, whereas the SNR increases clockwise. The standard deviation of the signal is 1.25^k for $k = 0, \ldots, 7$. Errors were generated from white noise with a standard deviation of 10 by first applying an AR(1) model with parameter 0.3 and following convolution with a Gaussian kernel with full-widths-half-maximum (FWHM) bandwidths $(1, 1, 0.5)$ times voxel size.
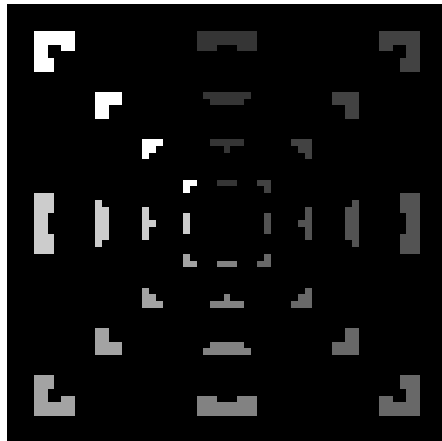

Figure 2: Location of activated regions and size of the signal within slices with activations for the artificial data set. Eight different signal-to-noise ratios, increasing clockwise, are coded by gray values. Black corresponds to the absence of a signal.
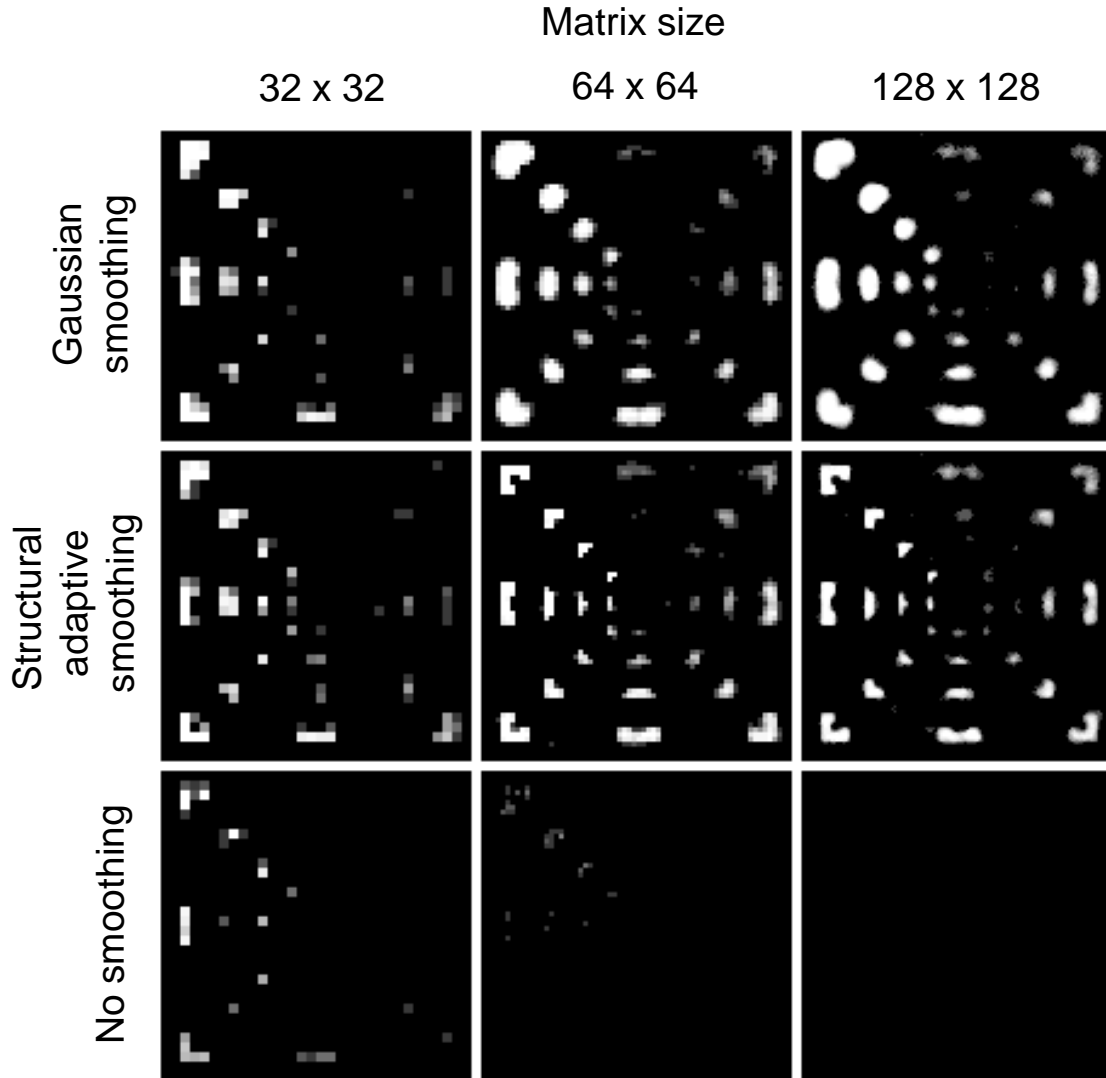
In order to simulate measurements at different spatial resolutions, we re-created the phantom at $32 \times 32 \times 26$, and $128 \times 128 \times 26$ voxels, through averaging and replicating the signal to the new resolution, respectively. Corresponding to our general setting in this paper Δz is held constant. At the lower resolution this automatically leads to partial volume effects since the original phantom was produced at the medium resolution. At the higher resolution the structures are larger than the voxel size. Independent noise has been added to all datasets. According to Eq. (3) with $32 \times 32 \times 26$ the standard deviation of the noise was divided by 2 compared to the value σ of the medium resolution; for $128 \times 128 \times 26$ the standard deviation is 2σ. This mimics the ratio of $1 : 2$ for the SNR in the absence of physiological noise and a constant FOV.

Figure 3: Probability of signal detection in an artificial dataset at different spatial resolutions in xy-plane as described in the text. The columns of this figure correspond to the three different spatial resolutions mimicking matrix sizes of 32×32, 64×64, and 128×128. The lower row is the signal detection result without smoothing. The middle row is the result of our structural adaptive smoothing procedure compared to classical Gaussian filter in the upper row.

The upper and middle rows in Figure 3 show voxelwise detection probabilities after smoothing the SPM with a Gaussian filter and with structural adaptive smoothing in contrast to no smoothing in the lower row. using a FWHM bandwidth of 1.5, 3, and 6 voxel sizes to achieve the same amount of smoothness in mm. The gray level corresponds to the relative frequency of signal detection obtained by averaging over all slices that contain activations. Signals from small areas with very low SNR ratio are practically not detected by either method. With Gaussian filtering the shapes of the detected activation areas
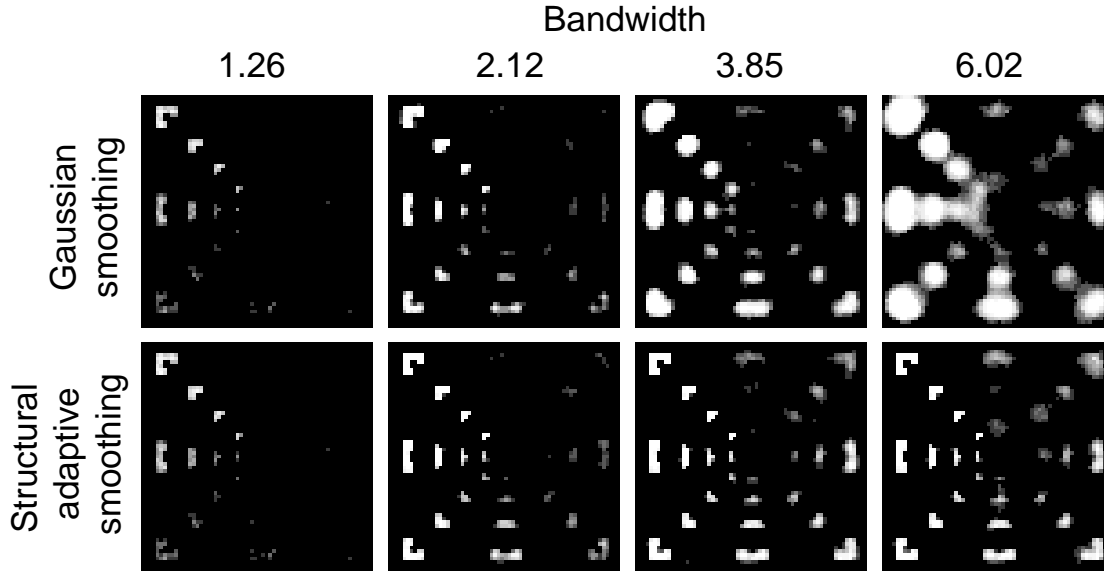
9

Figure 4: Dependency of the probability of signal detection on the maximum bandwidth of the algorithm for non-adaptive (upper row) and structural adaptive smoothing (lower row) at constant resolution. The bandwidth increases from left to right: 1.26, 2.12, 3.85, and 6.02. The resolution is the medium one of the artificial example (64×64).

are not well reproduced. In particular, concave structures are oversmoothed. In contrast to this result, the signal detection after smoothing with structural adaptive smoothing achieves a similar sensitivity but preserves the shape and size of activation areas.

Partial volume effects make it practically impossible to detect fine structure in the low resolution image, although the lower noise level would permit a voxelwise analysis without smoothing. Increasing spatial resolution shows the full potential of the structural adaptive smoothing method. Gaussian filtering oversmooths and thus reduces the signal in activation areas leading to smaller sensitivity, whereas false positives occur due to oversmoothing the signal into non-activated areas. Structural adaptive smoothing can reveal the shape of activation areas much better at medium resolution. Further increasing the resolution leads to more noise, but due to the increased number of activated voxels, also to a better adaptation and thus a more or less constant level of signal detection.

Furthermore, we show in this artificial example that due to the edge conserving properties of the structural adaptive smoothing procedure, we can take further advantage from increasing the maximum bandwidth of the iterations [Tabelow et al., 2006]. While non-adaptive smoothing simply decreases the effective resolution, structural adaptive smoothing further increases the sensitivity without compromising the shape of activation areas (see Fig. 4).

4.2 Experimental data

We conducted a series of experiments to verify that the improvements by structural adaptive smoothing can be achieved also in experimental data. After reconstruction of the raw data and motion correction, the time series in each voxel were modeled by a linear model, with a design matrix specifying the explanatory variables including the task indicator function convolved with a hemodynamic response function template. Drift terms were modeled by polynomials. To account for temporal correlation, the data was whitened by using an AR(1) model. After voxelwise estimation of the parameters, structural adaptive smoothing was applied to the array of parameters of interest to significantly reduce the variance of the parameter estimates. Adaptive smoothing also allows to weaken the multiple test problem and enables to define thresholds for the test statistic. A map of t-statistics was obtained from the smoothed parameter map. Thresholds were then defined by random field theory. Data was processed using afni [Cox, 1996] and the package "fmri" for R (R foundation for Statistical Computing) [Polzehl and Tabelow, 2007, R Development Core Team, 2006].

Experiments were performed on healthy volunteers and approved by the Institutional Review Board of Weill Cornell Medical College. Data was acquired on a 3.0 T General Electric (Milwaukee, WI) Signa Excite MRI scanner, using two-dimensional gradient echo echo planar imaging pulse sequences (GE-EPI) on an eight-channel head receive-only coil. For stimulus presentation, an IFIS system (InVivo, Orland (FL)) with a video display was used. Anatomical high-resolution scans of the whole head were acquired using a sagittal 3D-MPRAGE sequence (kindly provided by Gary Glover, Stanford University, CA) with acquisition matrix size $256 \times 190 \times 110$, 24 cm FOV, 1.5 mm slice thickness, TI/TE/TR/TD = 725 / 1.772 / 8.604 / 1400 ms, flip angle 7°, and 2 Nex.

Experiment 1 (motor) A somatosensory motor task was performed by one male subject. For functional MRI, a GE-EPI sequence with TE/TR = 40/2000 ms was used and 20 axial slices of 4 mm thickness were acquired. We used a field-of-view of 24 cm with a matrix size of 64×64 and 128×128, yielding voxel dimensions of 3.75 mm and 1.88 mm, respectively. A task was performed in three blocks of 60 s duration; each block consisted of 30 s task and 30 s rest. The first 4 scans before these block were discarded, yielding in total 105 scans. The task consisted of bimanual tapping of the thumb against all fingers of same hand, one by one and in quick succession. Note, that the setting for the higher resolution in accordance with Table 1 lead to a larger scan time per volume.

The analysis results at both resolutions after applying a Gaussian filter and structural adaptive smoothing are shown in Fig. 4.
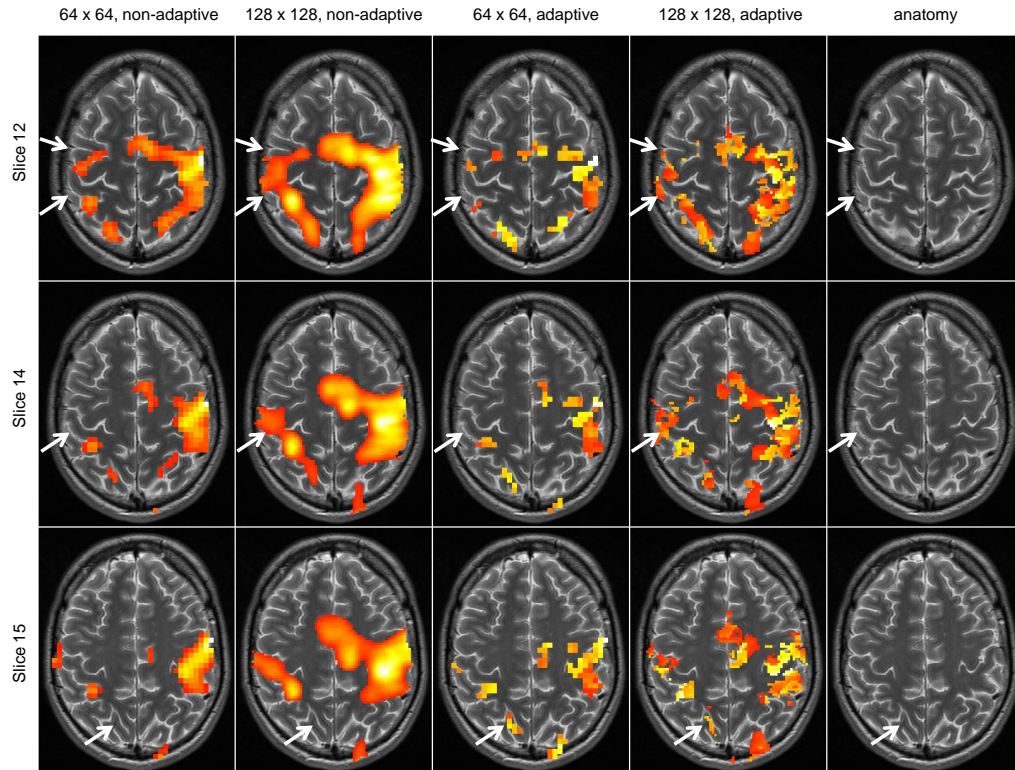
11

Figure 5: Three slices through the primary motor area, with matrix size and smoothing method of (left to right) 64×64 non-adaptive, 128×128 non-adaptive, 64×64 adaptive, 128×128 adaptive, anatomy. (Multiple test corrected p = 0.05.) Arrows mark regions that become only visible in high-resolution images, some of them only in high-resolution images with structural adaptive smoothing.

One observes that (i) smoothing with a Gaussian filter does not yield any new information at the higher resolution; (ii) in the high resolution scan analyzed with structural adaptive smoothing, more details than in the low resolution scan, analyzed with the same method, can be seen. Therefore, the high-resolution scan, analyzed with structural adaptive smoothing, yields more detailed information about functional activity than the low-resolution scan analyzed with either method.

Experiment 2 (visual) A visual experiment was performed on three subjects (one male and two females). For functional MRI, a GE-EPI sequence with TE/TR = 30/1500 ms was used, which sampled the signal also during the gradient ramps. 20 Slices of 4.5 mm thickness and a FOV of 22 cm were acquired. The matrix size was 64×64, 64×128 (zero filled to 128×128), and 128×128, yielding voxel dimensions of 3.44 mm, 1.72 mm,

and 1.72 mm, respectively. The varying scan time per volume was balanced by different coverage for the three acquisitions leading to 27, 19, and 16 slices, respectively. A task was performed in 14 blocks of 9 s duration; each block consisted of 9 s rest and 9 s task. The first 4 scans before these block were discarded. The task consisted of looking at a binocular stimulus, a flashing checkerboard displayed in two rectangles symmetric to the midline.

EPI images were aligned to anatomical images with the help of field maps [Jezzard and Balaban, 1995], using a technique for the construction of field maps from multi-channel data. This method builds upon the insight that, although phases for different channels are independent, field maps for different channels can only deviate from each other by multiples of 2π, plus noise. This construction of field maps from multi-channel data is described in the following. Phase images were acquired by a 2D-SPGR pulse sequence (in-plane to the EPI scans, TE = 7.00 and 9.24 ms, TR = 35 ms, acquisition matrix size 256×256, flip angle = $30°$, 1 NEX). All eight individual phase images per slice, corresponding to the eight channels of the multi-channel head coil used, were acquired. Field maps were computed from all of these images and then combined such as to minimize noise: Each field map was weighted with the power in each image voxel and field map voxels deviating more than $\pi/4$ from the weighted mean field map voxel were discarded, as long as field map voxels were comprised of at least three single field map contributions. Field maps were slightly extrapolated to regions outside the brain, de-spiked, and smoothed with a Gaussian filter of 2 mm FWHM. The final registrations between unwarped EPI volumes and the skull-stripped field map magnitude volumes were calculated in two steps: First, the EPI volumes were aligned with the skull-stripped field map magnitude volume, masking out voxels with a signal-dropout larger than 10%. Then, the skull-stripped field map magnitude volume was matched to the skull-stripped MP-RAGE volume. The field map was computed using FSL with FUGUE [Smith et al., 2004, Jenkinson, 2001].

The SPM's of one subject and the three scan parameter settings after applying a Gaussian filter and structural adaptive smoothing are shown in Fig. 6. The results for the other two subjects are similar and not shown here.

One observes that (i) in general, smoothing increases the SNR, because the p-values for the detected signals appear to be increased in the smoothed images. Thus, in case of weaker signals, smoothing would be the only way to detect a signal at all. (ii) Gaussian smoothing is able to increase SNR, but at the cost of effective resolution. Thus, for Gaussian smoothing there is no advantage measuring at the higher resolution with the accompanying loss in SNR, as described before. However, with structural adaptive
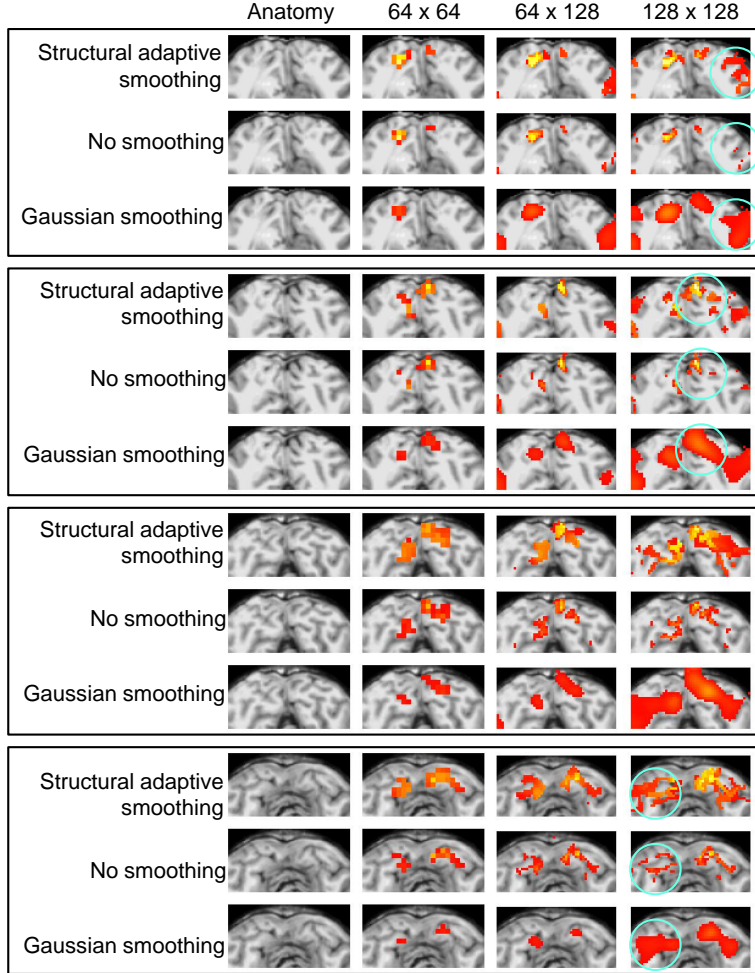
Figure 6: Signal detection in visual experiment at different spatial resolutions. Four subsequent slices in the visual cortex are shown. Columns from left to right: anatomical slice only, 64×64, 64×128, 128×128. upper row: structural adaptive smoothing, middle row: no smoothing, lower row: Gaussian smoothing. Some areas with distinct differences advantages of high-resolution images combined with structural adaptive smoothing are marked with circles.

smoothing the situation changes completely: (iii) For structural adaptive smoothing the detected activation areas nicely match the gray matter areas of the anatomical images. (iv) At the highest resolution, the benefits of structure adaptive smoothing become most pronounced.

In summary, we have shown that high-dimensional fMRI can be useful to detect the shape and location of activations more accurately than low-dimensional fMRI, in particular in

14

conjunction with structural adaptive smoothing. This methodology might allow one to tackle challenges of high-dimensional fMRI [Kriegeskorte and Bandettini, 2007a].

5   Discussion and Conclusion

Structural adaptive smoothing is capable to reveal finer activation structure in functional MRI at higher resolutions even when the lower SNR requires smoothing to detect signals at all. Therefore, structural adaptive smoothing enables one to better take advantage of higher resolution in functional imaging. We have shown that structural adaptive smoothing is able to detect signals at high acquisition resolution due to its edge preserving properties.

There are several advantages of acquiring functional data at higher resolutions. One advantage is the reduction of partial volume effects as they occur at low resolutions, which partly diminish the higher SNR at low resolution. Furthermore, low resolutions are too coarse for the recent interest of studying functional activation at a level of small scale organization such at cortical columns. Since the lower SNR is always against a decision for higher resolution, advanced smoothing methods such as structural adaptive smoothing can be a helpful tool to achieve this goal, in contrast to classical non-adaptive smoothing methods.

It has been shown before that smoothing in general can over-compensate for loss in time-course SNR of high resolution scans. The thorough study of [Triantafyllou et al., 2006] showed that in particular at very high fields (7.0 T) a high-resolution scan smoothed down to a normal resolution has an improved time-course SNR. This is by virtue of reducing physiological noise for the price of increased thermal noise, which is comparably low at these field strengths. In contrast, in our study we showed that it could be even advisable to scan with a high resolution and to retain this resolution during data processing, yielding an effectively higher resolution of statistical parametric maps. A word of caution is in place here: Smoothing methods as used here are blind against the origin of the signal variations; in another experiment that we performed (unpublished) about imaging ocular dominance columns in the visual cortex, structural adaptive smoothing of high-resolution scans also significantly increased spurious activation apparently related to motion, in particular near the interface between gray matter and cerebrospinal fluid. Since the temporal variability of such signals has distinct statistical properties it might be possible to identify and discard motion induced variability to some degree.

In addition to the proposed approach here, which is based on exploiting structural in-

fomation inherent in the EPI signal, there are at least two classes of complementary approaches to effectively increase the resolution of statistical parametric maps: Advances in imaging techniques to increase the sensitivity of the detection of the BOLD signal (for an overview, see [Harel et al., 2006]), advances in MRI scanner hardware, and anatomically informed methods. In the PS approach we did not take anatomical information as obtained from high-resolution anatomical images into account. Structure was extracted from the fMRI data itself. We therefore neglected the information on *anatomical structure* that is usually acquired in fMRI studies by high-resolution anatomical pulse sequences and then co-registered to the fMRI data. For example, the methods of cortical surface mapping [Andrade et al., 2001] and anatomically informed basis functions [Kiebel et al., 2000] increase the statistical significance of BOLD activations by restricting data evaluation to the cortical surface. [Flandin et al., 2002] use a cortex parcellation technique, which is believed to allow for relatively large spatial averaging informed by the anatomy and to provide an alternative to the solution of the multiple testing problem. The problem of automatically finding optimal parameters for the smoothing kernels and avoiding the mixing of information from distinct anatomical regions has been studied in [Grova et al., 2006]. The here proposed method should be seen as a complementary method to these anatomically informed procedures, as well as to other imaging techniques, and, if combined with them, might improve the accuracy of estimating statistical parametric maps further.

A similar heuristics as in the PS approach has been used by Lu et al. [Lu et al., 2003, Lu et al., 2004]. These authors identify clusters of activated voxels starting from seed voxels. In contrast, PS uses heuristics from scale space methods [Poline and Mazoyer, 1994, Siegmund and Worsley, 1995].

To summarize, with structural adaptive smoothing one can better utilize the advantages of functional MRI at higher resolutions.

Structure adaptive smoothing software used in this paper has been integrated into the "fmri" package in R [Polzehl and Tabelow, 2007, R Development Core Team, 2006].

Acknowledgments

References

[Andrade et al., 2001] Andrade, A. et al. (2001). Detection of fMRI activation using Cortical Surface Mapping. *Human Brain Mapping*, 12:79–93.

[Cox, 1996] Cox, R. (1996). Software for analysis and visualization of functional magnetic resonance neuroimages. *Computers and Biomed. Res.*, 29:162.

[Edelstein et al., 1986] Edelstein, W., Glover, G., Hardy, C., and Redington, R. (1986). The intrinsic signal-to-noise ratio in NMR imaging. *Magn. Reson. Med.*, 3(4):604–618.

[Flandin et al., 2002] Flandin, G., Kherif, F., Pennec, X., Malandain, G., Ayache, N., and Poline, J.-B. (2002). Improved detection sensitivity in functional MRI data using a brain parcelling technique. In *MICCAI (1)*, volume 2488, pages 467–474.

[Forman et al., 1995] Forman, S., Cohen, J., Fitzgerald, M., Eddy, W., Mintun, M., and Noll, D. (1995). Improved assessment of significant activation in functional magnetic resonance imaging (fMRI): use of a cluster-size threshold. *Magn. Reson. Med.*, 33:636–647.

[Friston et al., 1995] Friston, K., Holmes, A., Worsley, K., Poline, J.-B., Frith, C., and Frackowiak, R. (1995). Statistical parametric maps in functional imaging: A general linear approach. *Human Brain Mapping*, 2:189–210.

[Grova et al., 2006] Grova, C. et al. (2006). Anatomically informed interpolation of fMRI data on the cortical surface. *Neuroimage*, 31:1475–1486.

[Harel et al., 2006] Harel, N., Ugurbil, K., Uludag, K., and Yacoub, E. (2006). Frontiers of brain mapping using MRI. *J. Magn. Res. Imaging*, 23:945–957.

[Harrison et al., 2007] Harrison, L., Penny, W., Ashburner, Trujillo-Barreto, N., and Friston, K. (2007). Diffusion-based spatial priors for imaging. *NeuroImage*, 38:677–95.

[Harrison et al., 2008] Harrison, L., Penny, W., Daunizeau, J., and Friston, K. (2008). Diffusion-based spatial priors for functional magnetic resonance images. *Neuroimage*, 41:408–423.

[Jenkinson, 2001] Jenkinson, M. (2001). Improved unwarping of EPI images using regularised B0 maps. *NeuroImage*, 13(6):S165.

[Jezzard and Balaban, 1995] Jezzard, P. and Balaban, R. S. (1995). Correction for geometric distortion echo planar images from B_0 field variations. *Magn. Res. Med.*, 34:65–73.

[Kiebel et al., 2000] Kiebel, S. J., Goebel, R., and Friston, K. J. (2000). Anatomically informed basis functions. *Neuroimage*, 11:656–667.

[Kleinschmidt, 2007] Kleinschmidt, A. (2007). Different analysis solutions for different spatial resolutions? Moving towards a mesoscopic mapping of functional architecture in the human brain. *NeuroImage*, 38(4):663–665.

[Kriegeskorte and Bandettini, 2007a] Kriegeskorte, N. and Bandettini, P. (2007a). Analyzing for information, not activation, to exploit high-resolutiuon fMRI. *NeuroImage*, 38(4):649–662.

[Kriegeskorte and Bandettini, 2007b] Kriegeskorte, N. and Bandettini, P. (2007b). Combining tools: Activation- and information-based fMRI analysis. *NeuroImage*, 38(4):666–668.

[Krüger and Glover, 2001] Krüger, G. and Glover, G. (2001). Physiological noise in oxygenation-sensitive magnetic resonance imaging. *Magn. Reson. Med.*, 46:631–637.

[Lowe and Sorenson, 1997] Lowe, M. and Sorenson, J. (1997). Spatially filtering functional magnetic resonance imaging data. *Magn. Reson. Med.*, 37:723–729.

[Lu et al., 2003] Lu, Y., Jiang, T., and Zang, Y. (2003). Region growing method for the analysis of functional MRI data. *Neuroimage*, 20:455–465.

[Lu et al., 2004] Lu, Y., Jiang, T., and Zang, Y. (2004). Split-merge based region growing method for fMRI activation detection. *Human Brain Mapping*, 22:271–279.

[Parker and Gullberg, 1990] Parker, D. and Gullberg, G. (1990). Signal-to-noise efficiency in magnetic resonance imaging. *Med Phys*, 17(2):250–257.

[Poline and Mazoyer, 1994] Poline, J. B. and Mazoyer, B. M. (1994). Enhanced detection in brain activation maps using a multifiltering approach. *Journal of Cerebral Blood Flow and Metabolism*, 14:639–42.

[Polzehl and Spokoiny, 2001] Polzehl, J. and Spokoiny, V. (2001). Functional and dynamic magnetic resonance imaging using vector adaptive weights smoothing. *J. Roy. Statist. Soc. Ser. C*, 50:485–501.

[Polzehl and Spokoiny, 2006] Polzehl, J. and Spokoiny, V. (2006). Propagation-separation approach for local likelihood estimation. *Probab. Theory and Relat. Fields*, 135:335–362.

[Polzehl and Tabelow, 2007] Polzehl, J. and Tabelow, K. (2007). fmri: A package for analyzing fmri data. *RNews*, 7(2):13–17.

[R Development Core Team, 2006] R Development Core Team (2006). *R: A Language and Environment for Statistical Computing*. R Foundation for Statistical Computing, Vienna, Austria. ISBN 3-900051-07-0.

[Scouten et al., 2006] Scouten, A., Papademetris, X., and Constable, R. (2006). Spatial resolution, signal-to-noise ratio, and smoothing in multi-subject functional MRI studies. *NeuroImage*, 30(3):787–793.

[Siegmund and Worsley, 1995] Siegmund, D. O. and Worsley, K. J. (1995). Testing for a signal with unknown location and scale in a stationary Gaussian random field. *Ann. Statist.*, 23:608–639.

[Sijbers, 1998] Sijbers, J. (1998). *Signal and Noise Estimation from Magnetic Resonance Images*. PhD thesis, Universiteit Antwerpen.

[Smith et al., 2004] Smith, S. et al. (2004). Advances in functional and structural MR image analysis and implementation as FSL. *NeuroImage*, 23(S1):208–219.

[Tabelow et al., 2008] Tabelow, K., Polzehl, J., Ulug, A. M., Dyke, J. P., Heier, L. A., and Voss, H. U. (2008). Accurate localization of functional brain activity using structure adaptive smoothing. *IEEE Trans. Med. Imaging*, 27(4):531–537.

[Tabelow et al., 2006] Tabelow, K., Polzehl, J., Voss, H. U., and Spokoiny, V. (2006). Analyzing fMRI experiments with structural adaptive smoothing procedures. *NeuroImage*, 33(1):55–62.

[Triantafyllou et al., 2005] Triantafyllou, C., Hoge, R., Krüger, G., Wiggins, C., Potthast, A., Wiggins, G., and Wald, L. (2005). Comparison of physiological noise at 1.5 T, 3 T and 7 T and optimization of fMRI acquisition parameters. *NeuroImage*, 26(1):243–250.

[Triantafyllou et al., 2006] Triantafyllou, C., Hoge, R., and Wald, L. (2006). Effect of spatial smoothing on physiological noise in high-resolution fMRI. *NeuroImage*, 32(2):551–557.

[Worsley and Friston, 1995] Worsley, K. and Friston, K. (1995). Analysis of fMRI time series revisited - again. *NeuroImage*, 2:173–181.

[Worsley et al., 2002] Worsley, K., Liao, C., Aston, J. A. D., Petre, V., Duncan, G., Morales, F., and Evans, A. (2002). A general statistical analysis for fMRI data. *NeuroImage*, 15:1–15.